LBL-38601
UC-405
Preprint

Lawrence Berkeley Laboratory
UNIVERSITY OF CALIFORNIA

Submitted to *Journal of Nuclear Medicine*

Smoothing the Rough Edges of Tomographic Regions of Interest: An Approach to Variance Reduction

A. Kuruc and R.H. Huesman

April 1996

Donner Laboratory
Biology & Medicine Division

REFERENCE COPY
Does Not
Circulate
Bldg. 50 Library.
LBL-38601
Copy 1

Prepared for the U.S. Department of Energy under Contract Number DE-AC03-76SF00098

DISCLAIMER

This document was prepared as an account of work sponsored by the United States Government. While this document is believed to contain correct information, neither the United States Government nor any agency thereof, nor the Regents of the University of California, nor any of their employees, makes any warranty, express or implied, or assumes any legal responsibility for the accuracy, completeness, or usefulness of any information, apparatus, product, or process disclosed, or represents that its use would not infringe privately owned rights. Reference herein to any specific commercial product, process, or service by its trade name, trademark, manufacturer, or otherwise, does not necessarily constitute or imply its endorsement, recommendation, or favoring by the United States Government or any agency thereof, or the Regents of the University of California. The views and opinions of authors expressed herein do not necessarily state or reflect those of the United States Government or any agency thereof or the Regents of the University of California.

Smoothing the Rough Edges of Tomographic Regions of Interest: An Approach to Variance Reduction

Alvin Kuruc, M.D., Ph.D. and Ronald H. Huesman, Ph.D.
Center for Functional Imaging
Lawrence Berkeley National Laboratory
University of California, Berkeley, CA

April 16, 1996

Running head: Smoothing the Edges of Tomographic ROIs

Address for correspondence and reprints:
Ronald H. Huesman
MS 55-121
Lawrence Berkeley National Laboratory
University of California
1 Cyclotron Road
Berkeley, CA 94720

RHHuesman@lbl.gov
(510) 486-4062
(510) 486-4768 (FAX)

This work was supported in part by the Director, Office of Energy Research, Office of Health and Environmental Research, Medical Applications and Biophysical Research Division of the U.S. Department of Energy under contract No. DE-AC03-76SF00098 and in part by National Heart, Lung, and Blood Institute of the U.S. Department of Health and Human Services under grants T32-HL07367, P01-HL25840, and R01-HL50663.

Abstract

The standard procedure for estimating regional tracer concentrations from emission tomographic data may be summarized as follows. A region of interest (ROI) is defined within the organ of interest. The concentration estimate is obtained by integrating the reconstructed image over the ROI and dividing by the volume of the ROI. This estimate may be written as $\int \mathsf{m}(\mathbf{x})\hat{\mathsf{f}}(\mathbf{x})\,d\mathbf{x}$, where m is the normalized mask function of the ROI and $\hat{\mathsf{f}}$ is the reconstructed image. The purpose of this study was to investigate whether the variance of such tracer concentration estimates can be reduced by replacing the mask function m with a smoother function, termed an aperture function, that is 0 outside the ROI and whose integral is 1. The latter conditions insure that the resulting concentration estimate is unbiased.

Methods: We computed the variance of tracer concentration estimates using the conventional mask function as well as an appropriate aperture function for an idealized mathematical model of emission tomography as well as for real emission tomographic data collected from a phantom.

Results: In both the mathematical model and the phantom experiments, estimates obtained using an appropriate aperture function had a smaller variance than those obtained using the standard mask function.

Conclusion: The variance of regional tracer concentration estimates obtained from emission tomographic data can be reduced by replacing the usual mask function with a smoother aperture function.

Keywords: Emission tomography, Region of interest, Aperture function, Signal-to-noise, Quantitation.

1 Introduction

The standard procedure for estimating regional tracer concentrations in a target organ from emission tomographic data can be summarized as follows. A region of interest (ROI) is defined within the organ of interest. The concentration estimate is then obtained by integrating the reconstructed image over the ROI and dividing by the volume of the ROI. Let m denote the normalized mask function of the ROI, i.e.,

$$\mathsf{m}(\mathbf{x}) \equiv \begin{cases} 1/\,\text{volume(ROI)} & \text{if } \mathbf{x} \in \text{ROI} \\ 0 & \text{if } \mathbf{x} \notin \text{ROI} \end{cases},$$

and let $\hat{\mathsf{f}}$ denote the reconstructed estimate of the image f. Then the standard concentration estimate can be written as

$$\int \mathsf{m}(\mathbf{x})\hat{\mathsf{f}}(\mathbf{x})\, d\mathbf{x}. \tag{1.1}$$

Suppose that the tracer density in the ROI is equal to a constant, f_0, and that $\hat{\mathsf{f}}$ is an unbiased estimate of the true underlying image density f. Then it is easy to see that the expected value of the estimate given in equation 1.1 is equal to f_0, and hence our estimate is unbiased. Moreover, if the mask function m in equation 1.1 is replaced by a function $\mathsf{a}(\mathbf{x})$ that is uniformly 0 outside the ROI and of unit integral, our estimate is still unbiased. Thus, assuming f is constant within the ROI, one can construct many distinct unbiased estimators for the tracer density. The main point of this paper is that, due to the correlation properties of the statistical errors in reconstructed tomographic images, the variance of tracer concentration estimates can be reduced by replacing the normalized mask function m with a smoother function a. We term the function $\mathsf{a}(\mathbf{x})$ an aperture function. We shall see that this effect is intimately related to the tomographic nature of the observations; it does not occur in the analogous non-tomographic planar-imaging problem.

2 Methods

While emission tomography (ET) is inherently a 3-dimensional (3D) problem, it gives insight to begin by considering tomography in 2 dimensions. We therefore start by considering the effect of replacing the normalized mask function for a 2-dimensional (2D) ROI with an appropriate aperture function.

2.1 The 2D Problem

2.1.1 Mathematical Model for 2D ET

We consider a simple mathematical model of 2D ET. The model is highly idealized in that it ignores numerous secondary physical effects, such as attenuation and scatter, that occur in practice. However, it abstracts the basic problem of ET.

We identify the "image" with a probability density function, $\mathsf{f}(\mathbf{x})$, on the unit radius disk $D \subseteq \mathbb{R}^2$, where $\mathbb{R}^2$ denotes 2-dimensional Euclidean space. The locations of radioactive disintegrations are modeled as independent, identically distributed random variables distributed according to f. Denote the set of lines in $\mathbb{R}^2$ by $\mathbb{L}$. $\mathbb{L}$ is the observation or sinogram space. $\mathbb{L}$ is parameterized by assigning the coordinates (θ, s) to the line through $(s\cos\theta, s\sin\theta) \in \mathbb{R}^2$ perpendicular to the vector $(\cos\theta, \sin\theta)$. The observations in ET are modeled as independent, identically distributed random variables distributed according to the Radon transform of f, which we denote by $\mathsf{Rf}(\theta, s)$. For a given line $\mathbf{l} \in \mathbb{L}$, $\mathsf{Rf}(\mathbf{l})$ is defined to be the integral of f over $\mathbf{l}$.

We consider the statistical properties of regional tracer density estimates of the form $\int_{\mathbb{R}^2} \mathsf{a}(\mathbf{x})\hat{\mathsf{f}}(\mathbf{x})\,d\mathbf{x}$, where $\hat{\mathsf{f}}$ is the usual filtered-backprojection estimate of the underlying image f. One approach to obtaining these statistical properties is through Monte Carlo simulation. However, we believe that more

insight is obtained by computing the statistical properties of these estimates directly using what we term the observation-domain representation of these estimators.

2.1.2 Observation-Domain Representation of Estimators

It is shown in appendix A that the density estimate $\int_{\mathbb{R}^2} \mathsf{a}(\mathbf{x})\hat{\mathsf{f}}(\mathbf{x})\,d\mathbf{x}$ can be expressed as $n^{-1}\sum_{i=1}^{n} \mathsf{HRa}(\mathbf{l}_i)$, where $\mathbf{l}_1, \ldots, \mathbf{l}_n \in \mathbb{L}$ denote the observations in ET and H denotes the ramp-filter operator used in the filtered backprojection algorithm, cf. equation A.4. (H is defined more precisely in appendix A.) We see that our estimate may be expressed as the average value of the function HRa at the observation points. We call the function HRa an observation-domain representation of the estimator generated by a.

Our primary motivation for introducing observation-domain representations of estimators is that it makes their statistical analysis transparent. Since the observations are independent and identically distributed according to Rf, the expected value of our estimator is equal to

$$\int_{\mathbb{L}} \mathsf{HRa}(\mathbf{l})\mathsf{Rf}(\mathbf{l})\,d\mathbf{l} \equiv \pi^{-1}\int_0^{\pi}\int_{-\infty}^{\infty} \mathsf{HRa}(\theta, s)\mathsf{Rf}(\theta, s)\,ds\,d\theta$$

It is shown below in equation A.5 that

$$\int_{\mathbb{L}} \mathsf{HRa}(\mathbf{l})\mathsf{Rf}(\mathbf{l})\,d\mathbf{l} = \int_{\mathbb{R}^2} \mathsf{a}(\mathbf{x})\mathsf{f}(\mathbf{x})\,d\mathbf{x}.$$

Denoting the observation-domain representation of a by $\mathsf{b} \equiv \mathsf{HRa}$, a routine calculation shows that the variance of the estimator is given by

$$n^{-1}\left[\int_{\mathbb{L}} \mathsf{b}^2(\mathbf{l})\mathsf{Rf}(\mathbf{l})\,d\mathbf{l} - \left(\int_{\mathbb{L}} \mathsf{b}(\mathbf{l})\mathsf{Rf}(\mathbf{l})\,d\mathbf{l}\right)^2\right]. \tag{2.1}$$

Now let f_0 denote the assumed constant value of f on the ROI. Under the assumptions that the aperture function a vanishes outside the ROI and $\int_{\mathbb{R}^2} \mathsf{a}(\mathbf{x})\,d\mathbf{x} = 1$, the expression for the estimator mean reduces to f_0. It is thus an unbiased estimator of the tracer density.

2.1.3 Observation-Domain Representation of Mask Functions

There is a technical problem in applying the formulation in the preceding subsection to the case where a is a normalized mask function since the integral defining HRa does not converge. To fix this problem, it is customary to replace the operator H with a bandlimited substitute $\mathsf{H}_{\eta_{\max}}$ whose action is given by convolution with a function $h_{\eta_{\max}}$ on $\mathbb{L}$ whose Fourier transform with respect to the s variable is given by

$$\tilde{h}_{\eta_{\max}}(\theta,\eta) \equiv \begin{cases} \pi|\eta| & |\eta| \leq \eta_{\max} \\ 0 & |\eta| > \eta_{\max} \end{cases} .$$

Explicit formulas for evaluating the function $h_{\eta_{\max}}$ may be found in [1].

2.1.4 ROI and Aperture Functions

As an example, we consider the problem of estimating the regional tracer concentration inside an ROI consisting of a disk of radius $\rho = 0.25$ centered at the origin. As a smoother aperture function for this ROI, we used a Kaiser-Bessel function with support on the disk of radius ρ:

$$\mathsf{k}_\rho(\mathbf{x}) \equiv \begin{cases} \frac{\alpha I_0\{\alpha[1-(|\mathbf{x}|/\rho)^2]^{1/2}\}}{2\pi\rho^2 I_1(\alpha)} & |\mathbf{x}| \leq \rho \\ 0 & |\mathbf{x}| > \rho \end{cases} , \tag{2.2}$$

where I_i denotes the modified Bessel function of order i [2]. The parameter α was set equal to 2.25. The normalized mask function and the corresponding Kaiser-Bessel aperture function are illustrated in figure 1. The Kaiser-Bessel function was chosen because its Fourier transform is highly concentrated around the origin. This tends to mitigate the tendency of the ramp filter to amplify high-frequency noise.

It may be easily verified that the observation-domain representation of a radially symmetric function is independent of the θ variable and hence may

be written as an even function of the s variable. We will henceforth express these representations as functions of s alone.

2.1.5 Numerical Calculation of Estimator Variances

Numerical evaluation of estimator variances was done in the following way. Since both the image density f and the aperture function a were always taken to be radially symmetric, equation 2.1 for the variance reduces to

$$n^{-1}\left[\int_{-1}^{1} \mathsf{b}^2(s)\mathsf{Rf}(s)\,ds - \left(\int_{-1}^{1} \mathsf{b}(s)\mathsf{Rf}(s)\,ds\right)^2\right], \tag{2.3}$$

where we also used the fact that Rf vanishes outside the interval $[-1,1]$. We produced a sampled version of b as follows. The Radon transform of a was computed analytically. $\mathsf{Ra}(s)$ was sampled at p evenly spaced points about the origin with a sampling interval of $2/p$. Ramp filtering was done with a bandlimited ramp filter with $\eta_{\max}$ equal to the Nyquist frequency of $p/4$ cycles per unit length. $\mathsf{H}_{\eta_{\max}}$ was applied by discrete convolution of the sampled versions of $h_{\eta_{\max}}$ and b. The convolution was performed in the frequency domain using the Fast Fourier transform with appropriate zero padding.

To complete the numerical calculation of variances, $\mathsf{Rf}(s)$ was computed analytically and sampled at the same points as b was sampled. The integrals in equation 2.3 were then approximated by appropriate Riemann sums. For example,

$$\int_{-1}^{1} \mathsf{b}(s)\mathsf{Rf}(s)\,ds \approx (2/p)\sum_{i=1}^{p} b(s_i)Rf(s_i),$$

with $s_i \equiv (2i-p-1)/p$.

2.1.6 The Planar-Imaging Problem

It is instructive to compare the tomographic imaging problem, where the observations are distributed according to Rf, with the simpler non-tomographic

problem where the observations are distributed according to f itself. We term the latter problem the planar-imaging problem. The analogous estimate for $\int_{\mathbb{R}^2} \mathsf{a}(\mathbf{x})\mathsf{f}(\mathbf{x})\,d\mathbf{x}$ is $n^{-1}\sum_{i=1}^{n} \mathsf{a}(\mathbf{x}_i)$, where the $\mathbf{x}_i \in \mathbb{R}^2$ denote the observations. The expected value of this estimate is $\int_{\mathbb{R}^2} \mathsf{a}(\mathbf{x})\mathsf{f}(\mathbf{x})\,d\mathbf{x}$. The variance of this estimate is

$$n^{-1}\int_{\mathbb{R}^2}\left(\mathsf{a}(\mathbf{x})-\int_{\mathbb{R}^2}\mathsf{a}(\mathbf{x})\mathsf{f}(\mathbf{x})\,d\mathbf{x}\right)^2\mathsf{f}(\mathbf{x})\,d\mathbf{x}.$$

If $\mathsf{f} = f_0$ on the ROI, then $\int_{\mathbb{R}^2} \mathsf{a}(\mathbf{x})\mathsf{f}(\mathbf{x})\,d\mathbf{x} = f_0$ and the estimator is unbiased. Under the assumption that the aperture function a is of unit integral and vanishes outside the ROI, the expression for the variance then reduces to

$$\begin{aligned} n^{-1}\int_{\mathbb{R}^2}(\mathsf{a}(\mathbf{x})-f_0)^2\,\mathsf{f}(\mathbf{x})\,d\mathbf{x} &= n^{-1}\int_{\mathbb{R}^2}\left(\mathsf{a}^2(\mathbf{x})-2f_0\mathsf{a}(\mathbf{x})+f_0^2\right)\mathsf{f}(\mathbf{x})\,d\mathbf{x} \\ &= n^{-1}f_0\left(\int_{\mathrm{ROI}}\mathsf{a}^2(\mathbf{x})\,d\mathbf{x}-f_0\right). \end{aligned}$$

Denote the area of the ROI by A. We shall now show that among all aperture functions a satisfying the unbiasedness conditions $\mathsf{a} = 0$ outside the ROI and $\int_{\mathbb{R}^2} \mathsf{a}(\mathbf{x})\,d\mathbf{x} = 1$, the variance is minimized by the normalized mask function $\mathsf{a}(\mathbf{x}) = A^{-1}$ on the ROI. Indeed, writing the expression for the variance as

$$\begin{aligned} &n^{-1}f_0\left(\int_{\mathrm{ROI}}\mathsf{a}^2(\mathbf{x})\,d\mathbf{x}-f_0\right) \\ &= n^{-1}f_0\left(\int_{\mathrm{ROI}}\left(\mathsf{a}(\mathbf{x})-A^{-1}+A^{-1}\right)^2 d\mathbf{x}-f_0\right) \\ &= n^{-1}f_0\left(\int_{\mathrm{ROI}}\left(\mathsf{a}(\mathbf{x})-A^{-1}\right)^2 d\mathbf{x}\right. \\ &\qquad \left.+2A^{-1}\int_{\mathrm{ROI}}\left(\mathsf{a}(\mathbf{x})-A^{-1}\right)d\mathbf{x}+A^{-1}-f_0\right) \qquad (2.4) \\ &= n^{-1}f_0\left(\int_{\mathrm{ROI}}\left(\mathsf{a}(\mathbf{x})-A^{-1}\right)^2 d\mathbf{x}+A^{-1}-f_0\right), \qquad (2.5) \end{aligned}$$

it is obvious that the expression is minimized by choosing $\mathsf{a}(\mathbf{x}) = A^{-1}$, giving a variance of

$$f_0(A^{-1}-f_0)n^{-1}. \qquad (2.6)$$

2.2 The 3D Problem

The ideas developed in the analysis of tomography in 2D extend in a natural way to tomography in 3D. Quantitatively, the reduction in variance obtained by the choice of an appropriate aperture function can be greater in 3D than 2D. Our goal here is to exhibit this effect by means of a simple example.

For simplicity, we only consider the problem where a 3D cylindrical volume is reconstructed by combining 2D slices that are independently reconstructed from lines that are perpendicular to the axis of the cylinder. This is the usual case in practical imaging situations. While our methodology could be extended in a straightforward way to include more general imaging situations, such as positron volume imaging, we will not consider such problems here.

2.2.1 Mathematical Model for 3D ET

We identify the "image" with a probability density function, f, on a cylinder $C \subseteq \mathbb{R}^3$ of unit radius and unit height centered at the origin. We take the axis of the cylinder to coincide with the z axis in $\mathbb{R}^3$. The locations of radioactive disintegrations are modeled as independent, identically distributed random variables distributed according to f. Denote the set of lines in $\mathbb{R}^3$ parallel to the x-y plane by $\mathbb{Z}$. $\mathbb{Z}$ is the observation space. $\mathbb{Z}$ is parameterized by assigning the coordinates (θ, s, z) to the line through $(s\cos\theta, s\sin\theta, z) \in \mathbb{R}^3$ that is parallel to the x-y plane and perpendicular to the vector $(\cos\theta, \sin\theta, z)$. It will be convenient to define the plane in $\mathbb{R}^3$ with third coordinate z by $\mathbb{R}^2_z$ and the set of lines in $\mathbb{R}^2_z$ by $\mathbb{L}_z$. We will sometimes refer to the $\mathbb{R}^2_z$ as slices. The observations are modeled as independent, identically distributed $\mathbb{Z}$-valued random variables distributed according to Tf, where $\mathsf{Tf}(\theta, s, z)$ is equal to the 2D Radon transform of f restricted to $\mathbb{R}^2_z$. Denoting the restriction of f to $\mathbb{R}^2_z$ by f_z, we can write this as $\mathsf{Tf}(\theta, s, z) = \mathsf{Rf}_z(\theta, s)$.

We consider the statistical properties of regional tracer density estimates of the form $\int_{\mathbb{R}^3} \mathsf{a}(\mathbf{x})\hat{\mathsf{f}}(\mathbf{x})\,d\mathbf{x}$, where $\hat{\mathsf{f}}$ is the usual filtered-backprojection estimate of the underlying image f, i.e., for each z, $\hat{\mathsf{f}}_z$ is reconstructed on $\mathbb{R}^2_z$ from the lines in $\mathbb{L}_z$ using $2D$ filtered backprojection.

2.2.2 Observation-Domain Representation of Estimators

The observation-domain representation of the estimator generated by a is obtained simply by separately computing the $2D$ observation-domain representations of a restricted to each slice. In other words, an object domain representation of a is given by $\mathsf{b}(\theta, s, z) \equiv \mathsf{HRa}_z(\theta, s)$, where a_z denotes the restriction of a to $\mathbb{R}^2_z$. This follows from the 2D results since

$$\begin{aligned}
\int_{\mathbb{R}^3} \mathsf{a}(\mathbf{x})\hat{\mathsf{f}}(\mathbf{x})\,d\mathbf{x} &= \int_{\mathbb{R}}\int_{\mathbb{R}^2} \mathsf{a}_z(\mathbf{x})\hat{\mathsf{f}}_z(\mathbf{x})\,d\mathbf{x}\,dz \\
&= \int_{\mathbb{R}} n^{-1}\sum_{i=1}^{n} \mathsf{HRa}_z(\theta_i, s_i)\,\delta(z - z_i)\,dz \\
&= n^{-1}\sum_{i=1}^{n} \mathsf{b}(\mathbf{l}_i),
\end{aligned}$$

where δ denotes the Dirac delta function and (θ_i, s_i, z_i) denotes the coordinates of the ith observation. It now follows easily that the expected value of the estimator is

$$\begin{aligned}
\int_{\mathbb{Z}} \mathsf{b}(\mathbf{l})\mathsf{Tf}(\mathbf{l})\,d\mathbf{l} &= \int_{\mathbb{R}}\int_{\mathbb{L}} \mathsf{HRa}_z(\mathbf{l})\mathsf{Rf}_z(\mathbf{l})\,d\mathbf{l}\,dz \\
&= \int_{\mathbb{R}}\int_{\mathbb{R}^2} \mathsf{a}_z(\mathbf{x})\mathsf{f}_z(\mathbf{x})\,d\mathbf{x}\,dz \\
&= \int_{\mathbb{R}^3} \mathsf{a}(\mathbf{x})\mathsf{f}(\mathbf{x})\,d\mathbf{x}.
\end{aligned}$$

Under the assumption that $\mathsf{f} = f_0$ on the ROI and that $\mathsf{a} = 0$ outside the ROI and $\int_{\mathbb{R}^3} \mathsf{a}(\mathbf{x})\,d\mathbf{x} = 1$, the expected value is f_0. A routine calculation shows that

the variance of the estimator is given by

$$n^{-1}\left[\int_{\mathbb{Z}} [\mathsf{b}(\mathbf{l}) - f_0]^2\, \mathsf{Tf}(\mathbf{l})\, d\mathbf{l}\right].$$

In the 3D problem considered here, where each slice is reconstructed separately, it is useful to view the concentration estimate as a weighted average of independent concentration estimates from each slice. Writing our estimate as

$$\begin{aligned}&\int_{\mathbb{R}} n^{-1}\sum_{i=1}^{n} \mathsf{HRa}_z(\theta_i, s_i)\delta(z - z_i)\, dz \\ &= \int_{\mathbb{R}} n^{-1}\sum_{i=1}^{n} \frac{\mathsf{HRa}_z(\theta_i, s_i)}{\int_{\mathbb{R}^2} \mathsf{a}_z(\mathbf{x})\, d\mathbf{x}}\delta(z - z_i)\left(\int_{\mathbb{R}^2} \mathsf{a}_z(\mathbf{x})\, d\mathbf{x}\right) dz, \qquad (2.7)\end{aligned}$$

note that the function $\mathsf{HRa}_z / \int_{\mathbb{R}^2} \mathsf{a}_z(\mathbf{x})\, d\mathbf{x}$ generates an unbiased estimator for the density on the intersection of the ROI with the slice $\mathbb{R}^2_z$. These estimates are weighted according to the mass of the aperture function on each slice.

2.2.3 A More Efficient Estimator

In general, it is possible to reduce the variance of the estimate given by equation 2.7 by replacing the weights $\int_{\mathbb{R}^2} \mathsf{a}_z(\mathbf{x})\, d\mathbf{x}$ with more general weights $\mathsf{w}(z)$. We thus consider estimates of the form

$$\int_{\mathbb{R}} n^{-1}\sum_{i=1}^{n} \frac{\mathsf{HRa}_z(\theta_i, s_i)}{\int_{\mathbb{R}^2} \mathsf{a}_z(\mathbf{x})\, d\mathbf{x}}\delta(z - z_i)\mathsf{w}(z)\, dz.$$

It is clear that as long as these weights satisfy $\int_{\mathbb{R}} \mathsf{w}(z)\, dz = 1$, then the estimate will remain unbiased. The variance of this estimate is

$$n^{-1}\int_{\mathbb{R}}\int_{\mathbb{L}} \left(\frac{\mathsf{HRa}_z(\mathbf{l})}{\int_{\mathbb{R}^2} \mathsf{a}_z(\mathbf{x})\, d\mathbf{x}} - f_0\right)^2 \mathsf{Rf}_z(\mathbf{l})\, d\mathbf{l}\, \mathsf{w}^2(z)\, dz.$$

It is convenient to introduce some notation. First, we note that $\int_{\mathbb{L}} \mathsf{Rf}_z(\mathbf{l})\, d\mathbf{l}$ is just the marginal probability density of z under the probability density Tf.

By elementary properties of the Radon transform, this is equal to the marginal probability density of z under the probability density f. We thus define

$$\begin{aligned}\mathsf{f}_m(z) &= \int_{\mathbb{R}^2} \mathsf{f}_z(\mathbf{x})\,d\mathbf{x} \\ &= \int_{\mathbb{L}} \mathsf{Rf}_z(\mathbf{l})\,d\mathbf{l}.\end{aligned}$$

Using this definition, we can rewrite the expression for the variance as

$$n^{-1}\int_{\mathbb{R}}\int_{\mathbb{L}}\left(\frac{\mathsf{HRa}_z(\mathbf{l})}{\int_{\mathbb{R}^2}\mathsf{a}_z(\mathbf{x})\,d\mathbf{x}} - f_0\right)^2 \frac{\mathsf{Rf}_z(\mathbf{l})}{\mathsf{f}_m(z)}\,d\mathbf{l}\,\mathsf{f}_m(z)\,\mathsf{w}^2(z)\,dz. \tag{2.8}$$

Second, we note that

$$\frac{\mathsf{Rf}_z(\mathbf{l})}{\mathsf{f}_m(z)}$$

is just the conditional probability density of the observations given z. It follows that

$$\int_{\mathbb{L}}\left(\frac{\mathsf{HRa}_z(\mathbf{l})}{\int_{\mathbb{R}^2}\mathsf{a}_z(\mathbf{x})\,d\mathbf{x}} - f_0\right)^2 \frac{\mathsf{Rf}_z(\mathbf{l})}{\mathsf{f}_m(z)}\,d\mathbf{l}$$

is just the conditional variance given z of the estimator generated by b. We shall denote this variance by $\sigma^2_{\text{cond}}(z)$. Substituting this notation into equation 2.8 gives a variance of

$$n^{-1}\int_{\mathbb{R}}\sigma^2_{\text{cond}}(z)\mathsf{f}_m(z)\mathsf{w}^2(z)\,dz. \tag{2.9}$$

In appendix B, we show that, subject to the unbiasedness constraint $\int_{\mathbb{R}}\mathsf{w}(z)\,dz = 1$, the expression for the variance given in equation 2.9 is minimized by setting

$$\mathsf{w}(z) = \frac{[\sigma^2_{\text{cond}}(z)\mathsf{f}_m(z)]^{-1}}{\int_{\mathbb{R}}[\sigma^2_{\text{cond}}(z)\mathsf{f}_m(z)]^{-1}\,dz}.$$

This result is analogous to the well-known result of elementary statistics that statistically independent estimates should be weighted inversely to their variance to minimize the variance of the combined estimate [3, sec. 3.5].

2.2.4 3D Example

As an example, we considered the problem of estimating the regional tracer concentration inside an ROI consisting of a sphere of radius $\rho = 0.25$ centered at the origin. As an aperture function for this ROI, we used

$$\mathsf{a}(\mathbf{x}) = \begin{cases} \mathsf{k}_{(\rho^2-z^2)^{1/2}}(x,y) \cdot \frac{\rho^2-z^2}{\frac{4}{3}\pi\rho^3} & |\mathbf{x}| \leq \rho \\ 0 & |\mathbf{x}| > \rho \end{cases}, \tag{2.10}$$

where $\mathsf{k}_{(\rho^2-z^2)^{1/2}}$ is the 2D Kaiser-Bessel function defined in equation 2.2. The weighting in z was chosen to be identical to the weighting in z of the normalized mask function of the ROI. We also considered the minimum-variance weighted derived in section 2.2.3. We assumed that the underlying distribution of activity is uniform throughout the cylinder and that each slice is reconstructed independently using the standard filtered backprojection algorithm.

2.2.5 Numerical Calculation of Estimator Variances

Numerical evaluation of estimator variances was done using essentially the same procedure used in the $2D$ problem. The only difference was that the functions b and Tf also needed to be sampled in z. This was done by sampling at $p/2$ evenly spaced points about the origin with a sampling interval of $2/p$.

2.3 2D Problem Phantom Experiment

We attempted to verify our simulation results by conducting a phantom experiment on a real tomograph. We scanned a uniform cylindrical phantom containing approximately 60 MBq of germanium-68 distributed in a solid polyurethane matrix and encased in a high-density polyethylene cylinder (CTI Services, Inc., Nashville, TN). The phantom was approximately 22 cm in diameter and 23 cm in length. Scans were performed on the Donner 600 Crystal

Positron Tomograph [4].

We collected a total of 600 30-second sinograms. The sinograms were organized into 300 angular projections each consisting of 201 bins, cf. [5]. The sinograms were corrected for crystal-pair efficiency based on a preceding scan of a rotating rod source [6] and corrected for photon attenuation based on a transmission scan of the phantom. The implementation of these corrections was similar to that described in [5]. Images were reconstructed on a 256×256 grid using the filtered backprojection algorithm with a band-limited ramp filter whose cutoff frequency was set equal to the Nyquist frequency as described in section 2.1.3. The image grid size was $2/\pi$ times the bin size.

We considered the amount of tracer in a circular ROI centered at the center of the phantom with a radius of 0.25 times that of the phantom. For an aperture function for this region, we used the Kaiser-Bessel aperture function given in equation 2.2 with $\alpha = 2.25$.

For each frame, we computed the density estimate generated by the normalized mask function for the ROI and the aperture function. The sample mean, m, and variance, s^2, of these estimates over the 600 frames was then computed. The standard errors of these statistics were estimated by $s/\sqrt{n}$ and $\sqrt{2}s^2/\sqrt{n}$, respectively [7, sec. 10.15]. Results were expressed as statistic$\pm$standard error. The statistical significance of the difference between the means and variances was computed using Student's t-test and the F-test, respectively. Since the theory predicted that the means should be equal, but the variance of the functional generated by the aperture function should be less than that of the functional generated by the ROI, a two-tailed test was used for the means, while a one-tailed test was used for the variances. The threshold of statistical significance was set equal to $P = 0.05$.

3 Results

3.1 2D Simulation Results

For the 2D problem, we considered a circular ROI of radius $\rho = 0.25$ and took the image f to be the uniform density on the unit disk D, i.e., $\mathsf{f} = \pi^{-1}$. ET results were computed for $p = 128$ sample points.

3.1.1 Planar Imaging

For the uniform distribution, $f_0 = \pi^{-1}$. The area of the ROI is $A = \pi\rho^2$. Thus the expression for the variance of the estimator generated by the normalized mask function given by equation 2.6 evaluates to

$$\begin{aligned} \pi^{-2}(\rho^{-2} - 1)n^{-1} &= 15\pi^{-2}n^{-1} \\ &\approx 1.52n^{-1}. \end{aligned}$$

The variance of the estimator generated by the aperture function k_ρ was $1.65n^{-1}$. Thus the RMS signal-to-noise ratios are $0.26n^{1/2}$ and $0.25n^{1/2}$ for m and k_ρ, respectively.

3.1.2 Results for ET

The observation-domain representations of the estimators generated by m and k_ρ are shown in figure 2. For a uniform distribution of tracer on D, the variance of the estimate generated by the mask function m was $18.0n^{-1}$. The variance of the estimate generated by the aperture function k_ρ was $14.3n^{-1}$. Since the true tracer concentration was π^{-1}, the RMS signal-to-noise ratios were $7.5 \times 10^{-2}n^{1/2}$ and $8.4 \times 10^{-2}n^{1/2}$, respectively.

With equation 2.3 in mind, one sees from figure 2 that, roughly speaking, the reduction in variance obtained using the aperture function k_ρ in place of

the normalized mask function m is due to a reduction in the negative peaks just outside the central region.

3.2 3D Simulation Results

For the 3D problem, we considered a spherical ROI of radius $\rho = 0.25$ centered at the origin and took the image f to be the uniform density on cylinder C, i.e., $\mathsf{f} = \pi^{-1}$. ET results were computed for $p = 128$ sample points.

3.2.1 Results for ET

For the case of a uniform underlying distribution of tracer on C, the variance of the estimate generated by the mask function m was $61.0n^{-1}$. The variance of the estimate generated by the aperture function a in equation 2.10 was $49.7n^{-1}$. Since the true tracer concentration was π^{-1}, the RMS signal-to-noise ratios were $4.07 \times 10^{-2}n^{1/2}$ and $4.50 \times 10^{-2}n^{1/2}$, respectively.

When the weighting in z was modified to the minimum variance weighting, the estimators generated by m and a had variances of $58.8n^{-1}$ and $47.9n^{-1}$, respectively. The RMS signal-to-noise ratios increased to $4.15 \times 10^{-2}n^{1/2}$ and $4.60 \times 10^{-2}n^{1/2}$, respectively.

3.3 2D Phantom Results

The mean values for the estimates generated by the ROI and the aperture functions were $(3.003 \pm 0.010) \times 10^5$ and $(2.996 \pm 0.009) \times 10^5$, respectively. The difference between the means was not statistically significant ($P > 0.08$). The variance for these estimates was $(5.60 \pm 0.32) \times 10^8$ and $(4.63 \pm 0.27) \times 10^8$, respectively. Thus the variance for the estimate generated by the ROI was 1.21 times that for the estimate generated by the aperture function. This difference was statistically significant ($P = 0.01$).

4 Discussion

Our results indicate that a small, but significant, reduction in the variance of tracer concentration estimates may be obtained by simply replacing the usual mask function with a smoother aperture function. For example, our results for the 3D problem give a variance that is 78% of the variance of the usual estimator. This translates to a 22% reduction in imaging time or radiation dose while attaining equivalent statistical information.

Lewitt has advocated the replacement of the traditional voxels by Kaiser-Bessel aperture functions in iterative reconstruction algorithms [8]. Simulation results have indicated that this replacement can improve image quantification [9]. It seems plausible that this improvement, at least in part, is due to the variance reduction effect described in this paper. Moreover, quantification of the variance reduction effect may give a good metric for choosing an appropriate aperture function.

There are some applications in which the assumption that the tracer density is constant throughout the ROI is almost certainly valid. One example is measurement of tracer concentration in blood using an ROI within the left ventricular cavity of the heart. In most applications, this will only be approximately true. If the tracer concentration is not constant over the ROI, the two approaches may give somewhat different results. Roughly speaking, the concentration estimates obtained using the new procedure will be weighted more toward the center of the organ. The significance of this point will depend on the particular application. It likely will have the beneficial effect of reducing the effect of contamination from nearby organs.

The RMS signal-to-noise ratio found for the normalized mask function in the 2D problem roughly agrees with previously obtained empirical results on the statistical uncertainty in reconstructed tomographic images [10] [11]. For

example, Budinger et al. [11, eq. 11] claims the RMS SNR in a pixel is given by $\approx m^{-3/4}n^{1/2}/1.2$, where m is the total number of pixels and n is the total number of observations. If we equate the total number of pixels to the inverse of the relative area of a circular ROI, this predicts a RMS SNR of $\approx 0.83\rho^{3/2}n^{1/2}$ for an ROI of radius ρ. For $\rho = 0.25$, this amounts to $0.104n^{1/2}$, which is in rough agreement with our result of $0.084n^{1/2}$.

The result mentioned in the preceding paragraph that RMS SNR for a 2D circular ROI of radius ρ is approximately proportional to $\rho^{3/2}$ gives some insight into the difference between the estimator generated by the normalized mask function in 3D and the one with the optimized weights derived in section 2.2.3. Consider the problem of estimating the tracer density inside a 3D sphere. In the estimator generated by the normalized mask function, the concentration estimates from the slices are weighted according to the area of their intersection with the ROI; if the radius of this intersection is ρ, the weight is proportional to ρ^2. However, the RMS SNR being approximately proportional to $\rho^{3/2}$ implies that the optimal weights are approximately proportional to ρ^3.

For an irregularly shaped ROI, an appropriate aperture function may be constructed as follows. Let $\mathsf{d}(\mathbf{x})$ denote the distance from a point x in the image space to the exterior of the ROI. One then composes an aperture function for a circular ROI of radius $\rho = \max_{\mathbf{x}\in\mathrm{ROI}} \mathsf{d}(\mathbf{x})$ with the function $\mathsf{d} - \rho$.

In our examples, we only considered cases where the underlying distribution is uniform. In practice, it will be desirable to optimize the aperture function for the underlying distribution. This is straightforward to do since an estimate of the variance for a given aperture function can be obtained simply by replacing Rf in equation 2.1 with the measured observation density. In essence, this equation reflects the uncertainty in the observations due to counting statistics. More generally, it will also be desirable to modify this expression to reflect the

additional uncertainty introduced by preprocessing to correct for attenuation and other secondary physical effects.

A Observation-Domain Representation of Estimators

The standard filtered-backprojection reconstruction algorithm is based on the inversion formula for the Radon transform

$$\mathsf{f} = \mathsf{R}^T \mathsf{H} \mathsf{R} \mathsf{f}, \tag{A.1}$$

where R^T and H denote the backprojection and ramp-filter operators, respectively [12, thm. II.2.1]. The backprojection operator, which takes functions on $\mathbb{L}$ to functions on $\mathbb{R}^2$, is given explicitly by

$$\mathsf{R}^T \mathsf{g}(\mathbf{x}) \equiv \pi^{-1} \int_0^\pi \mathsf{g}(\theta, \theta \cdot \mathbf{x})\, d\theta,$$

where $\theta \equiv (\cos\theta, \sin\theta)$ and $\cdot$ denotes dot product. The notation R^T is used to indicate that R^T is the adjoint operator of R, i.e., it satisfies the equality

$$\int_{\mathbb{L}} \mathsf{R}\mathsf{f}(\mathbf{l})\mathsf{g}(\mathbf{l})\, d\mathbf{l} \equiv \pi^{-1} \int_0^\pi \int_{\mathbb{R}} \mathsf{R}\mathsf{f}(\theta, s)\mathsf{g}(\theta, s)\, ds\, d\theta = \int_{\mathbb{R}^2} \mathsf{f}(\mathbf{x})\mathsf{R}^T\mathsf{g}(\mathbf{x})\, d\mathbf{x}, \tag{A.2}$$

for all functions f on $\mathbb{R}^2$ and g on $\mathbb{L}$ [12, eq. II.1.7]. (The matrix analogue of the adjoint operator is the transpose. The matrix analogue of equation A.2 is the matrix identity $\mathbf{C}\mathbf{a} \cdot \mathbf{b} = \mathbf{a} \cdot \mathbf{C}^T\mathbf{b}$.) The action of the ramp-filter operator H, which maps functions on $\mathbb{L}$ to functions on $\mathbb{L}$, may be described as follows. Define the function h on $\mathbb{L}$ by

$$\mathsf{h}(\theta, s) \equiv \pi \int_{\mathbb{R}} e^{i2\pi s\eta} |\eta|\, d\eta,$$

so that, for each θ, the Fourier transform of h with respect to the s variable is the ramp function $\pi|\eta|$. Then for each θ, $\mathsf{H}\mathsf{g}(\theta, s)$ is equal to the convolution of g and h with respect to the s variable. It may be verified that H is its own adjoint, i.e., it satisfies the equality

$$\int_{\mathbb{L}} \mathsf{H}\mathsf{g}(\mathbf{l})\mathsf{g}'(\mathbf{l})\, d\mathbf{l} = \int_{\mathbb{L}} \mathsf{g}(\mathbf{l})\mathsf{H}\mathsf{g}'(\mathbf{l})\, d\mathbf{l} \tag{A.3}$$

for all functions $\mathbf{g}$ and $\mathbf{g}'$ on $\mathbb{L}$.

The filtered backprojection estimate of f, $\hat{\mathsf{f}}$, may be obtained in following way. Let $\mathbf{l}_1, \ldots, \mathbf{l}_n \in \mathbb{L}$ denote the observations in ET and $\delta(\mathbf{l}_i)$ denote a unit point mass at $\mathbf{l}_i$. We estimate Rf by the empirical estimate $n^{-1}\sum_{i=1}^{n}\delta(\mathbf{l}_i)$. Substituting this estimate into equation A.1 gives the filtered backprojection estimate

$$\hat{\mathsf{f}} \equiv n^{-1}\sum_{i=1}^{n}\mathsf{R}^T\mathsf{H}\delta(\mathbf{l}_i)$$

of f. Substituting this expression into our concentration estimate and using the adjoint equations A.2 and A.3 for R and H gives

$$\begin{aligned}\int_{\mathbb{R}^2}\mathbf{a}(\mathbf{x})\hat{\mathsf{f}}(\mathbf{x})\,d\mathbf{x} &= n^{-1}\sum_{i=1}^{n}\int_{\mathbb{R}^2}\mathbf{a}(\mathbf{x})\mathsf{R}^T\mathsf{H}\delta(\mathbf{x})\,d\mathbf{x}\\ &= n^{-1}\sum_{i=1}^{n}\int_{\mathbb{L}}\mathsf{HRa}(\mathbf{l})\delta(\mathbf{l})\,d\mathbf{l}\\ &= n^{-1}\sum_{i=1}^{n}\mathsf{HRa}(\mathbf{l}_i). \qquad \text{(A.4)}\end{aligned}$$

We see that our estimate may be expressed as the average value of the function HRa at the observation points. We call the function HRa an observation-domain representation of the estimator generated by a. This result may be found in [13]. A discrete version may be found in [14].

Since the observations are independent and identically distributed according to Rf, the expected value of our estimator is equal to

$$\begin{aligned}\int_{\mathbb{L}}\mathsf{HRa}(\mathbf{l})\mathsf{Rf}(\mathbf{l})\,d\mathbf{l} &= \int_{\mathbb{R}^2}\mathsf{a}(\mathbf{x})\mathsf{R}^T\mathsf{HRf}(\mathbf{x})\,d\mathbf{x}\\ &= \int_{\mathbb{R}^2}\mathsf{a}(\mathbf{x})\mathsf{f}(\mathbf{x})\,d\mathbf{x}, \qquad \text{(A.5)}\end{aligned}$$

where we used the adjoint properties of R and H in the first equality and the inversion formula for the Radon transform in the second.

B Minimum Variance Weights for the 3D Problem

In this appendix, we show that, subject to the unbiasedness constraint

$$\int_{\mathbb{R}} \mathsf{w}(z)\, dz = 1,$$

the expression for the variance given in equation 2.9 is minimized by setting

$$\mathsf{w}(z) = \frac{[\sigma^2_{\text{cond}}(z)\mathsf{f}_m(z)]^{-1}}{\int_{\mathbb{R}}[\sigma^2_{\text{cond}}(z)\mathsf{f}_m(z)]^{-1}\, dz}.$$

Using the method of Lagrange multipliers, we set the derivative of the Lagrangian function

$$\int_{\mathbb{R}} \sigma^2_{\text{cond}}(z)\mathsf{f}_m(z)\mathsf{w}^2(z)\, dz + \lambda\left(\int_{\mathbb{R}} \mathsf{w}(z)\, dz - 1\right),$$

with respect to w equal to 0. This yields the equation

$$2\mathsf{w}(z)\sigma^2_{\text{cond}}(z)\mathsf{f}_m(z) + \lambda = 0.$$

The solution to this equation is

$$\mathsf{w}(z) = \frac{-\lambda}{2\sigma^2_{\text{cond}}(z)\mathsf{f}_m(z)}.$$

The Lagrange multiplier λ is determined from the constraint conditions:

$$\begin{aligned} 1 &= \int_{\mathbb{R}} \mathsf{w}(z)\, dz \\ &= \frac{-\lambda}{2}\int [\sigma^2_{\text{cond}}(z)\mathsf{f}_m(z)]^{-1}\, dz \\ \lambda &= \frac{-2}{\int_{\mathbb{R}}[\sigma^2_{\text{cond}}(z)\mathsf{f}_m(z)]^{-1}\, dz}. \end{aligned}$$

Thus the minimizing weights are

$$\mathsf{w}(z) = \frac{[\sigma^2_{\text{cond}}(z)\mathsf{f}_m(z)]^{-1}}{\int_{\mathbb{R}}[\sigma^2_{\text{cond}}(z)\mathsf{f}_m(z)]^{-1}\, dz}.$$

Acknowledgements

The authors thank Natasha Kusabov and Matt Ho for their help in acquiring the phantom studies and Greg Klein and Bryan Reutter for their advice and help with programming and data analysis. Bryan Reutter also gave many helpful comments on preliminary drafts of this manuscript. This work was supported in part by the Director, Office of Energy Research, Office of Health and Environmental Research, Medical Applications and Biophysical Research Division of the U.S. Department of Energy under contract No. DE-AC03-76SF00098 and in part by National Heart, Lung, and Blood Institute of the U.S. Department of Health and Human Services under grants T32-HL07367, P01-HL25840, and R01-HL50663.

References

[1] G. N. Ramachandran and A. V. Lakshminarayanan. Three-dimensional reconstruction of radiographs and electron micrographs: Application of convolutions instead of Fourier transforms. *Proc. Nat. Acad. Sci. USA*, 68:2236–2240, 1971.

[2] Robert M. Lewitt. Multidimensional digital image representations using generalized Kaiser-Bessel window functions. *J. Opt. Soc. Am. A*, 7:1834–1846, 1990.

[3] Gilbert Strang. *Linear Algebra and Its Applications.* Academic Press, New York, 1980.

[4] S. E. Derenzo, R. H. Huesman, J. L. Cahoon, A. Geyer, D. Uber, T. Vuletich, and T. F. Budinger. A positron tomograph with 600 BGO crystals and 2.6mm resolution. *IEEE Trans. Nucl. Sci.*, 35:659–664, 1988.

[5] R. H. Huesman and J. L. Cahoon. Data acquisition, reconstruction and display for the Donner 280-crystal positron tomograph. *IEEE Trans. Nucl. Sci.*, NS-27:474–478, 1980.

[6] R. H. Huesman, S. E. Derenzo, J. L. Cahoon, A. B. Geyer, W. W. Moses, D. C. Uber, T. Vuletich, and T. F. Budinger. Orbiting transmission source for positron tomography. *IEEE Trans. Nucl. Sci.*, 34:735–739, 1988.

[7] Maurice G. Kendall, Alan Stuart, and J. K. Ord. *Distribution Theory*, volume I of *Kendall's Advanced Theory of Statistics.* Oxford University Press, New York, fifth edition, 1987.

[8] R. M. Lewitt. Alternatives to voxels for image representation in iterative reconstruction algorithms. *Phys. Med. Biol.*, 37:705–716, 1992.

[9] S. Matej, G. T. Herman, T. K. Narayan, S. S. Furuie, R. M. Lewitt, and P. E. Kinahan. Evaluation of task-oriented performance of several fully 3D PET reconstruction algorithms. *Phys. Med. Biol.*, 39:355–367, 1994.

[10] R. H. Huesman. The effects of a finite number of projection angles and finite lateral sampling of projections on the propagation of statistical errors in transverse section reconstruction. *Phys. Med. Biol.*, 22:511–521, 1977.

[11] Thomas F. Budinger, Stephen E. Derenzo, Grant T. Gullberg, William L. Greenberg, and Ronald H. Huesman. Emission computer assisted tomography with single-photon and positron annihilation photon emitters. *J. Comput. Assist. Tomogr.*, 1:131–145, 1977.

[12] F. Natterer. *The Mathematics of Computed Tomography.* John Wiley & Sons, New York, 1986.

[13] P. J. Bickel and Y. Ritov. Estimating linear functionals of a PET image. *IEEE Trans. Med. Imaging*, 14:81–87, 1995.

[14] Ronald H. Huesman. A new fast algorithm for the evaluation of regions of interest and statistical uncertainly in computed tomography. *Phys. Med. Biol.*, 29:543–552, 1984.

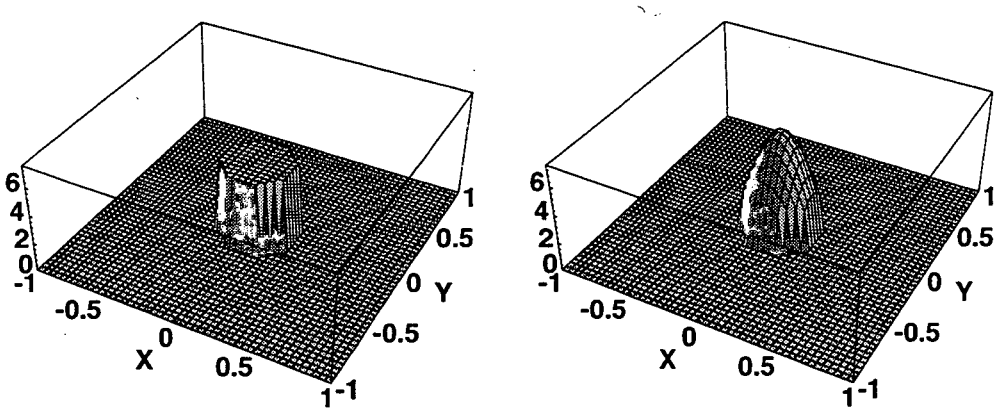

Figure 1: The normalized mask function m and Kaiser-Bessel aperture function k_ρ for a circular ROI of radius $\rho = 0.25$.

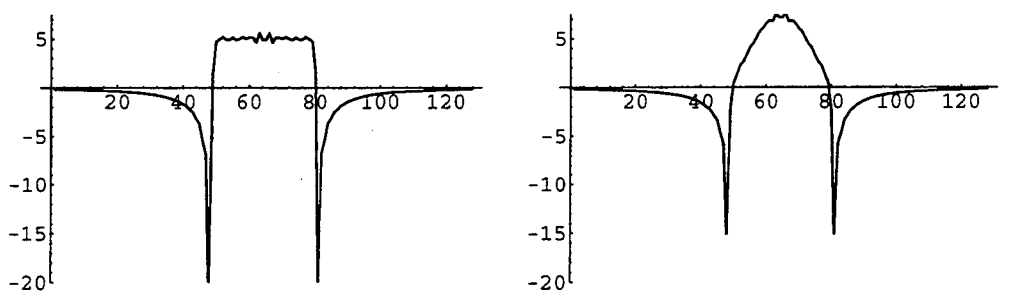

Figure 2: Observation-domain representations of the estimators generated by the functions shown in Figure 1.

LAWRENCE BERKELEY LABORATORY
UNIVERSITY OF CALIFORNIA
TECHNICAL INFORMATION DEPARTMENT
BERKELEY, CALIFORNIA 94720